Research in Astron. Astrophys. **2009** Vol. **9** No. **9**, 993–1010
*http://www.raa-journal.org* *http://www.iop.org/journals/raa*

***R**esearch in*
***A**stronomy and*
***A**strophysics*

# Multicolor photometric study of M31 globular clusters *

Zhou Fan[1,2], Jun Ma[1] and Xu Zhou[1]

[1] National Astronomical Observatories, Chinese Academy of Sciences, Beijing 100012, China; *fanzhou@bac.pku.edu.cn*
[2] Graduate University of Chinese Academy of Sciences, Beijing 100049, China

Received 2009 March 11; accepted 2009 June 8

**Abstract** We present the photometry of 30 globular clusters (GCs) and GC candidates in 15 intermediate-band filters covering the wavelength region from $\sim$ 3000 to $\sim$ 10 000 Å using the archival CCD images of M31 observed as part of the Beijing - Arizona - Taiwan - Connecticut (BATC) Multicolor Sky Survey. We transform these intermediate-band photometric data into the photometry in the standard $UBVRI$ broad-bands. These M31 GC candidates are selected from the Revised Bologna Catalog (RBC V.3.5), and most of these candidates do not have any photometric data. Therefore, the presented photometric data are a supplement to the RBC V.3.5. We find that 4 out of 61 GCs and GC candidates in RBC V.3.5 do not show any signal on the BATC images at their locations. By applying a linear fit of the distribution in the color-magnitude diagram of blue GCs and GC candidates using data from the RBC V.3.5, in this study, we find the "blue-tilt" of blue M31 GCs with a high confidence at 99.95% or $3.47\sigma$ for the confirmed GCs, and $> 99.99\%$ or $4.87\sigma$ for GCs and GC candidates.

**Key words:** galaxies: individual (M31) — galaxies: star clusters — galaxies: evolution

## 1 INTRODUCTION

Globular clusters (GCs) are the oldest bound stellar systems in galaxies, so they provide a fossil record of the earliest stages of galactic formation and evolution. In addition, since the GCs are bright ($\langle M_V \rangle < -7.5$), they can be detected over large distances such as in the Virgo (see, e.g., Peng et al. 2006) and Coma Clusters (see, e.g., Baum et al. 1995). Furthermore, Kalirai et al. (2008) discovered the GC system (GCS) of a galaxy which is ∼375 Mpc away ($z = 0.089$) and Mieske et al. (2004) detected a GCS in Abell 1689 ($z = 0.183$), both of which are based on deep image observations with the Advanced Camera for Surveys (ACS) on the *Hubble Space Telescope* (*HST*). We can study the evolutionary process of a distant galaxy through the nature of its GCs. Finally, GCs are helpful for studying a simple stellar population, since the populations in a GC are generally thought to have the same age and the same metallicity. However, some Galactic GCs, such as NGC 2808 and NGC 1851 are now suspected of being composed of heterogeneous populations, and recent data from *HST* are hinting at a great fraction of Galactic GCs being composite populations, at least chemically (see, e.g., Yi 2009 and references there).

Located at a distance of ∼780 kpc (see, e.g., Stanek & Garnavich 1998; Macri et al. 2001; McConnachie et al. 2005), M31 is the largest and nearest Sb-type spiral galaxy in the Local Group. According to the latest catalog: The Revised Bologna Catalog of M31 GCs and GC candidates (RBC

∗ Supported by the National Natural Science Foundation of China.

V.3.5) (Galleti et al. 2004; Galleti et al. 2006; Galleti et al. 2007), there are 509 confirmed GCs and 1058 GC candidates discovered in M31 so far and 421 former GC candidates have been proved to be stars, asterisms, galaxies, H II regions or extended clusters. These GCs and GC candidates in RBC were observed and discovered by many authors using different observation systems, i.e. CCD photometry, photoelectric photometry, and photographic plates, and a few are visual photometry (see, e.g., Vetesnik 1962; Sargent et al. 1977; Battistini et al. 1980; Crampton et al. 1985; Barmby et al. 2000). To obtain homogeneous photometric data, Galleti et al. (2004) took the photometric data of Barmby et al. (2000) as a reference and transformed others to this standard to make the Master Catalog RBC (see details in Galleti et al. 2004). Although this catalog includes the most comprehensive photometry so far, there are dozens of GCs and GC candidates having almost no photometric data. So, it is an impending task to present the photometry for these GCs and candidates.

In the present study, we will present the BATC multicolor photometric data for 30 GCs and GC candidates in RBC V.3.5, which have almost no photometric or spectroscopic information.

This paper is organized as follows. In Section 2, we present the BATC observations and Section 3 describes the data reduction process. In Section 4, the final photometric results are given and we compare our photometry to photometry in the literature. The new magnitude and color distributions of the M31 GCs and GC candidates are also shown in Section 4. Finally, concluding remarks are given in Section 5.

## 2 THE SAMPLE AND OBSERVATIONS

### 2.1 The Sample GC Candidates

To date, the study of M31 GCs has been mainly based on the comprehensive Bologna Catalog (Battistini et al. 1980, 1987, 1993). In particular, Galleti et al. (2004) collected and revised all the available photometry, obtaining homogeneous photometric data in the $UBVRI$ bands by comparing all the data with the CCD photometry of Barmby et al. (2000) as a reference. In addition, Galleti et al. (2004) searched the counterparts of the objects in their catalog based on the 2MASS database, providing integrated $J, H, K_s$ photometry for 529 GCs and GC candidates, of which no previous NIR photometry was observed. This catalog is referred to as the Revised Bologna Catalog of M31 globulars (hereafter RBC) (Galleti et al. 2004). It is worth mentioning that RBC is frequently revised (Galleti et al. 2004, 2005, 2006, 2007). The latest RBC was updated on March 27, 2008, and referred to as RBC V.3.5[1], which includes the newly discovered star clusters from Mackey et al. (2006), Kim et al. (2007) and Huxor et al. (2008). When we check the distribution of $V$ magnitudes in RBC V.3.5, we find that there are 61 GCs and GC candidates not having $V$ magnitudes, which are drawn in Figure 1 with open and solid circles. The solid circles represent the multicolor photometry of these GCs and GC candidates obtained in this paper. In fact, there are few photometric data in any filters for these objects. So, in order to obtain the photometry for these objects, we searched the BATC survey archive during 1995 February $-$ 2008 March, i.e., from the beginning to the end of M31 observations before 2008 March (since the M31 field cannot be observed at Xinglong Station after March every year), covering about 6 square degrees, as showed in Figure 1. There are 519 individual images extracted, of which the observation images during 1995 September $-$ 1999 December have been dealt with by Jiang et al. (2003) (see their table 1). There are 7 of them (EXT8, SH25, B306D, DAO11, BA22, BH01 and BA10) out of the BATC observation fields. So, the final sample of M31 GC candidates in this paper includes 54 objects. However, in this paper, we obtained the BATC multicolor photometry for 30 objects. The photometry for the other 24 objects are not obtained in this paper because of low signal-to-noise ratio or other reasons, which will be discussed in detail below. By comparing with tables 1, 3, 4 and 5 of Caldwell et al. (2009), who present a new catalog of 670 likely star clusters, stars, possible stars and galaxies in the field of M31, all with updated high-quality coordinates being accurate to $0.2''$ based on the images from the Local Group Survey (Massey et al. 2006) or Digitized Sky Survey (DSS), we find that, of these 54 objects, only four (V234, H13, B523 and SK131C) are not included in tables 1, 3, 4 and 5 of Caldwell et al. (2009). In addition, there are 5 objects, the coordinates of which are different between Galleti et al. (2004) (RBC

[1] Please see the details and download the catalog from *http://www.bo.astro.it/M31/*

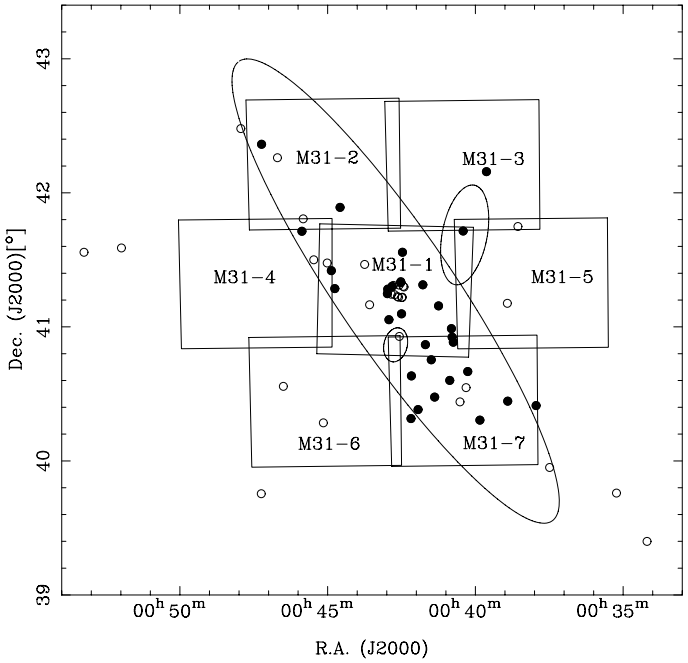


**Fig. 1** BATC observations of the M31 field and every field box is $58' \times 58'$ (for the old CCD). The large ellipse is the boundary of the disk and halo of M31 (Racine 1991). The other two small ellipses are $D_{25}$ of NGC 205 (northwest) and M32 (southeast). All the symbols (both open and solid) indicate 61 GCs and GC candidates not having $V$ magnitudes in RBC V.3.5, and the solid symbols represent that the multicolor photometry of these GCs and GC candidates are obtained in this paper.

V.3.5) and Caldwell et al. (2009). We listed them in Table 1 for comparison. Since Caldwell et al. (2009) corrected the coordinates of M31 clusters based on the Hectospec fibers and the FK5 system, we used the coordinates in Caldwell et al. (2009) to obtain the multicolor photometry for these five clusters in this paper.

Below, we will discuss the 24 objects in detail, the photometry of which were not obtained in this paper.

1. There are 13 GCs and GC candidates (B523, DAO32, NB27, NB31, NB35, NB43, NB59, NB62, NB84, NB85, DAO83, SK131C and V229), the signal-to-noise ratios of which are too low in the BATC survey images of this paper, therefore we do not obtain their photometry.
2. NB57, NB60, SH05 and SH08: In the BATC survey images of this paper, nothing was found on their positions given in RBC V.3.5. Maybe they are too faint to be seen in the BATC survey images. However, there is an object very near the position of NB60 presented by Galleti et al. (2004). The R.A. and DEC of this object are 00:42:26.63 and +41:18:04.5 compared to the R.A. and DEC of 00:42:26.68 and +41:18:10.70 presented by RBC V.3.5 for NB60.
3. B287: This cluster is very close to an object in the BATC survey images (because of the low resolution of the BATC system); the distance between the centers of these two objects is about 3 pixels in the BATC images (in fact, from the BATC images, these two objects join together), and we cannot obtain its photometry accurately in this paper.
4. B287D: It is very close to an object in the BATC survey images; the distance between the centers of these two objects is about 3 pixels in the BATC images, and we also cannot obtain its photometry accurately in this paper. In addition, this object is classified as a star by Caldwell et al. (2009).

5. B259D: This object is classified as a star by Caldwell et al. (2009). In addition, it overlaps another object in the BATC survey images. Therefore, we also did not obtain its photometry in this paper.
6. DAO88: This object is faint; the magnitude in the $V$ filter is $19.82\pm0.15$ from Caldwell et al. (2009). In addition, it is close to a much brighter star in the Milk Way (the magnitude of this star in the BATC $g$ filter is $12.23 \pm 0.002$). This star contaminates DAO88, although the distance between the centers of these two objects is 28 pixels in the BATC images, and we also cannot obtain its photometry accurately in this paper. In addition, the spectrum of this object is emission-line dominated from Caldwell et al. (2009).
7. H13 and V300: In the BATC survey images, these two objects both overlap another object, so we also did not obtain their photometry in this paper.
8. V254: It looks very extended in the BATC images, and is probably not a star cluster. In fact, Caldwell et al. (2009) has classified this object as an H II region. Thus, we do not present its multicolor photometry in this paper.

**Table 1** Comparison of the Coordinates from Caldwell et al. (2009). These five objects are from RBC V.3.5.

| | Caldwell et al. (2009) | | RBC V.3.5 | |
|---|---|---|---|---|
| ID | R.A. (J2000) | DEC. (J2000) | R.A. (J2000) | DEC. (J2000) |
| (1) | (2) | (3) | (4) | (5) |
| DAO23 | 00:38:54.19 | +40:26:33.9 | 00:38:54.34 | +40:26:46.4 |
| V203 | 00:40:47.80 | +40:59:06.0 | 00:40:48.62 | +40:59:11.4 |
| SH07 | 00:39:37.36 | +42:09:57.1 | 00:39:37.73 | +42:09:28.3 |
| V202 | 00:40:47.82 | +40:55:34.3 | 00:40:47.29 | +40:55:25.5 |
| DAO16 | 00:37:57.25 | +40:24:49.7 | 00:37:56.83 | +40:24:45.5 |

**Table 2** Comparison of the Two BATC CCDs

| Parameters (1) | Old CCD (2) | New E2V CCD (3) |
|---|---|---|
| Pixel Number | $2048 \times 2048$ | 4096×4096 |
| Spatial Scales | $1.67''$ pixel$^{-1}$ | $1.33''$ pixel$^{-1}$ |
| FOV | $58' \times 58'$ | $92' \times 92'$ |
| Blue Quantum Efficiency ( at 4000 Å) | $< 5\%$ | 92.2 % |
| Red Quantum Efficiency ( at 8500 Å) | $\sim 40\%$ | 59.4 % |

## 2.2 Observations

The observations of M31 were carried out by the BATC Multicolor Sky Survey System, which uses a 60/90 cm f/3 Schmidt telescope at Xinglong Station of the National Astronomical Observatories, Chinese Academy of Sciences (NAOC), where the typical seeing condition is $\sim\ 2'' - 3''$ (Ma et al. 2006a). This system includes 15 intermediate-band filters, covering a range of wavelengths from 3000 to 10 000 Å (e.g., Fan et al. 1996; Zhou et al. 2003). Before 2006 February, a Ford Aerospace $2\mathrm{k} \times 2\mathrm{k}$ thick CCD camera was applied, which has a pixel size of 15 $\mu$m and a field of view of $58'$ $\times\ 58'$, resulting in a resolution of $1.7''\mathrm{pixel}^{-1}$. Later, a new E2V $4\mathrm{k} \times 4\mathrm{k}$ thinned CCD with a pixel size of 12 $\mu$m, has successfully been mounted in the focal plane of the Schmidt telescope, resulting in a resolution of $1.3''\mathrm{pixel}^{-1}$. The blue quantum efficiency of the new E2V thinned CCD, which is $92.2\%$ at 4000 Å, is much higher than the old thick one. Please refer to Table 2 for a comparison of the parameters of thick and thinned CCDs.

**Table 3** BATC Obervational Log for M31–2 – M31–7 Fileds

| Field | Filter | Central Wavelength (Å) | Bandwidth (Å) | Image Number | Exposure (h) | Limiting Mags (S/N=5) (mag) |
|---|---|---|---|---|---|---|
| (1) | (2) | (3) | (4) | (5) | (6) | (7) |
| M31–2 | $a$ | 3360 | 222 | 7 | 2.1 | 19.63 |
| ... | $b$ | 3890 | 187 | 7 | 2.1 | 19.96 |
| ... | $c$ | 4210 | 185 | 4 | 0.8 | 20.05 |
| ... | $d$ | 4550 | 222 | 9 | 3.0 | 20.09 |
| ... | $e$ | 4920 | 225 | 3 | 1.0 | 19.53 |
| ... | $f$ | 5270 | 211 | 3 | 1.0 | 18.60 |
| ... | $g$ | 5795 | 176 | 3 | 1.0 | 19.32 |
| ... | $h$ | 6075 | 190 | 3 | 1.0 | 19.29 |
| ... | $i$ | 6660 | 312 | 5 | 1.7 | 20.47 |
| ... | $j$ | 7050 | 121 | 6 | 2.0 | 19.25 |
| ... | $k$ | 7490 | 125 | 4 | 1.3 | 18.83 |
| ... | $m$ | 8020 | 179 | 3 | 1.0 | 19.12 |
| ... | $n$ | 8480 | 152 | 5 | 1.7 | 18.10 |
| ... | $o$ | 9190 | 194 | 3 | 1.0 | 18.53 |
| ... | $p$ | 9745 | 188 | 5 | 1.7 | 16.83 |
| M31–3 | $a$ | 3360 | 222 | 7 | 2.1 | 17.55 |
| ... | $b$ | 3890 | 187 | 6 | 1.8 | 18.43 |
| ... | $c$ | 4210 | 185 | 4 | 1.0 | 20.08 |
| ... | $d$ | 4550 | 222 | 3 | 1.0 | 18.62 |
| ... | $e$ | 4920 | 225 | 4 | 1.3 | 19.76 |
| ... | $f$ | 5270 | 211 | 3 | 1.0 | 19.75 |
| ... | $g$ | 5795 | 176 | 3 | 1.0 | 19.50 |
| ... | $h$ | 6075 | 190 | 3 | 1.0 | 19.56 |
| ... | $i$ | 6660 | 312 | 3 | 1.0 | 18.10 |
| ... | $j$ | 7050 | 121 | 3 | 1.0 | 18.12 |
| ... | $k$ | 7490 | 125 | 3 | 1.0 | 19.47 |
| ... | $m$ | 8020 | 179 | 3 | 1.0 | 18.64 |
| ... | $n$ | 8480 | 152 | 8 | 2.7 | 17.89 |
| ... | $o$ | 9190 | 194 | 4 | 1.3 | 17.81 |
| ... | $p$ | 9745 | 188 | 7 | 2.3 | 17.92 |
| M31–4 | $a$ | 3360 | 222 | 6 | 1.8 | 17.41 |
| ... | $b$ | 3890 | 187 | 4 | 1.1 | 17.47 |
| ... | $c$ | 4210 | 185 | 6 | 1.5 | 18.02 |
| ... | $d$ | 4550 | 222 | 3 | 1.0 | 20.03 |
| ... | $e$ | 4920 | 225 | 3 | 1.0 | 20.25 |
| ... | $f$ | 5270 | 211 | 3 | 1.0 | 19.49 |
| ... | $g$ | 5795 | 176 | 3 | 1.0 | 19.93 |
| ... | $h$ | 6075 | 190 | 4 | 1.3 | 20.30 |
| ... | $i$ | 6660 | 312 | 3 | 1.0 | 19.55 |
| ... | $j$ | 7050 | 121 | 3 | 1.0 | 19.57 |
| ... | $k$ | 7490 | 125 | 3 | 1.0 | 19.40 |
| ... | $m$ | 8020 | 179 | 3 | 1.0 | 18.93 |
| ... | $n$ | 8480 | 152 | 5 | 1.7 | 17.68 |
| ... | $o$ | 9190 | 194 | 7 | 2.3 | 18.95 |
| ... | $p$ | 9745 | 188 | 3 | 1.0 | 16.71 |
| M31–5 | $a$ | 3360 | 222 | 6 | 2.0 | 16.54 |
| ... | $b$ | 3890 | 187 | 8 | 2.5 | 17.03 |
| ... | $c$ | 4210 | 185 | 7 | 1.8 | 20.50 |
| ... | $d$ | 4550 | 222 | 3 | 1.0 | 20.19 |
| ... | $e$ | 4920 | 225 | 3 | 1.0 | 19.49 |
| ... | $f$ | 5270 | 211 | 3 | 1.0 | 20.02 |
| ... | $g$ | 5795 | 176 | 3 | 1.0 | 20.03 |
| ... | $h$ | 6075 | 190 | 3 | 1.0 | 20.27 |
| ... | $i$ | 6660 | 312 | 3 | 1.0 | 20.07 |
| ... | $j$ | 7050 | 121 | 3 | 1.0 | 19.51 |
| ... | $k$ | 7490 | 125 | 3 | 1.0 | 19.35 |
| ... | $m$ | 8020 | 179 | 3 | 1.0 | 18.73 |

**Table 3** – *Continued.*

| Field | Filter | Central Wavelength (Å) | Bandwidth (Å) | Image Number | Exposure (h) | Limiting Mags (S/N=5) (mag) |
|---|---|---|---|---|---|---|
| (1) | (2) | (3) | (4) | (5) | (6) | (7) |
| ... | $n$ | 8480 | 152 | 6 | 2.0 | 18.21 |
| ... | $o$ | 9190 | 194 | 3 | 1.0 | 18.22 |
| ... | $p$ | 9745 | 188 | 6 | 2.0 | 18.33 |
| M31–6 | $a$ | 3360 | 222 | 7 | 2.1 | 17.43 |
| ... | $b$ | 3890 | 187 | 7 | 2.1 | 17.58 |
| ... | $c$ | 4210 | 185 | 7 | 1.8 | 17.70 |
| ... | $d$ | 4550 | 222 | 6 | 2.0 | 16.07 |
| ... | $e$ | 4920 | 225 | 4 | 1.3 | 19.62 |
| ... | $f$ | 5270 | 211 | 3 | 1.0 | 19.69 |
| ... | $g$ | 5795 | 176 | 3 | 1.0 | 19.22 |
| ... | $h$ | 6075 | 190 | 3 | 1.0 | 19.25 |
| ... | $i$ | 6660 | 312 | 6 | 2.0 | 19.83 |
| ... | $j$ | 7050 | 121 | 3 | 1.0 | 18.97 |
| ... | $k$ | 7490 | 125 | 3 | 1.0 | 17.24 |
| ... | $m$ | 8020 | 179 | 3 | 1.0 | 17.95 |
| ... | $n$ | 8480 | 152 | 5 | 1.7 | 17.50 |
| ... | $o$ | 9190 | 194 | 3 | 1.0 | 17.59 |
| ... | $p$ | 9745 | 188 | 6 | 2.0 | 18.22 |
| M31–7 | $a$ | 3360 | 222 | 6 | 2.0 | 19.66 |
| ... | $b$ | 3890 | 187 | 6 | 2.0 | 20.26 |
| ... | $c$ | 4210 | 185 | 3 | 0.8 | 15.49 |
| ... | $d$ | 4550 | 222 | 3 | 1.0 | 19.86 |
| ... | $e$ | 4920 | 225 | 3 | 1.0 | 20.16 |
| ... | $f$ | 5270 | 211 | 3 | 1.0 | 20.06 |
| ... | $g$ | 5795 | 176 | 3 | 1.0 | 19.24 |
| ... | $h$ | 6075 | 190 | 3 | 1.0 | 19.37 |
| ... | $i$ | 6660 | 312 | 3 | 1.0 | 19.99 |
| ... | $j$ | 7050 | 121 | 5 | 1.7 | 20.09 |
| ... | $k$ | 7490 | 125 | 3 | 1.0 | 17.73 |
| ... | $m$ | 8020 | 179 | 3 | 1.0 | 18.08 |
| ... | $n$ | 8480 | 152 | 6 | 2.0 | 18.28 |
| ... | $o$ | 9190 | 194 | 6 | 2.0 | 18.10 |
| ... | $p$ | 9745 | 188 | 6 | 2.0 | 17.92 |

M31 fields were observed in several observing runs: the first run was on the nights of UT 1995 February − 1999 December; the second observation was on the nights of UT 2004 January 12−27 and 2004 February 1−7; the third observation was on the nights of UT 2004 August 12−19, September 6−27 and October 1−12; the fourth observation was on the nights of UT 2005 October 31 and November 1−7; the fifth observation was on the nights of UT 2006 October 6−29 and November 1−18. Table 3 summarizes the observational catalog including the name of the observed field, filter name, central wavelength, width of filter, numbers of images combined, exposure time, and limiting magnitude, respectively.

Figure 1 shows the location of seven observed fields which are drawn with boxes, the names of which are labeled in each box. The total observed field of view is about six square degrees.

## 3 DATA REDUCTION AND PHOTOMETRY

Descriptions of the BATC photometric system can be found in Fan et al. (1996). Bias subtraction and flat-fielding with dome flats were done with the BATC automatic data reduction software, PIPELINE I, developed for the BATC Multicolor Sky Survey (Fan et al. 1996; Zheng et al. 1999). The dome flat-field images were taken by using a diffuser plate in front of the corrector plate of the Schmidt telescope, and the flat fielding technique has been verified (see e.g., Fan et al. 1996; Zheng et al. 1999;

Wu et al. 2002; Yan et al. 2000; Zhou et al. 2001, 2004). Spectrophotometric calibration of the M31 images were made by observations of four $F$ sub-dwarfs, HD 19445, HD 84937, BD $+26\,^{\circ}2606$ and BD $+17^{\circ}4708$, all taken from Oke & Gunn (1983). Hence, our magnitudes are defined in a way similar to the spectrophotometric AB magnitude system (i.e, the Oke & Gunn $\tilde{f_\nu}$ monochromatic system).

The BATC magnitudes (see, e.g., Yan et al. 2000; Zhou et al. 2001, 2003) of the AB magnitude system are defined as

$$m_{\rm BATC} = -2.5\log\frac{\int_{\lambda_1}^{\lambda_2} d(\log\nu) f_\nu r_\nu}{\int_{\lambda_1}^{\lambda_2} d(\log\nu) r_\nu} - 48.60, \quad (1)$$

which links the magnitude to the number of photons detected by the CCD rather than to the input flux (Fukugita et al. 1996). In Equation (1), $\nu$ is frequency; $f_\nu$ is the spectral energy distribution of the source in units of $\rm erg\,s^{-1}\,cm^{-2}\,Hz^{-1}$; $r_\nu$ is the filter response function of the system; and $\lambda_1$ and $\lambda_2$ are the lower and upper cutoff wavelengths of the passband, respectively.

### 3.1 Calibrations for $a$ and $b$ Intermediate-band Filters of the M31–1 Field

Jiang et al. (2003) and Ma et al. (2006b, 2006c, 2007) studied 203 M31 GCs and GC candidates based on the BATC observations in the $c$ to $p$ intermediate-band filters for the M31 central field (M31–1 in Fig. 1). In this paper, we also used the combined images and calibrated results of Jiang et al. (2003) to obtain the photometric data for our sample GCs and GC candidates in the intermediate-band filters of $c$ to $p$, which are in the M31–1 field. For the new observed images of the M31–1 field in $a$ and $b$ intermediate-band filters, we reduced them by automatic reduction software: Pipeline I, which includes bias subtraction and flat fielding of the CCD images. Then, we combined the images observed in the same filter to eliminate cosmic rays and to increase the signal-to-noise ratios as usually done in photometry. The absolute flux of the combined images was calibrated using the observations of standard stars (see, e.g., Fan et al. 1996; Zheng et al. 1999; Wu et al. 2002; Yan et al. 2000; Zhou et al. 2001, 2004).

Table 4 lists the observational parameters of the BATC M31–1 observed in the $a$ and $b$ filters: filter name, central wavelength, width of filter, numbers of combined images, exposure time, the calibration errors in magnitude of the standard stars, and limiting magnitude, respectively.

**Table 4** Parameters of the BATC Filters and Statistics of Observations in M31–1 Filed

| Filter | C.W.[a] (Å) | Bandwidth[b] (Å) | Image Number[c] | Exposure[d] (h) | Calibration Error[e] (mag) | Limiting Mags (S/N=5)[f] (mag) |
|---|---|---|---|---|---|---|
| (1) | (2) | (3) | (4) | (5) | (6) | (7) |
| $a$ | 3360 | 222 | 6 | 1.5 | 0.018 | 19.88 |
| $b$ | 3890 | 187 | 6 | 2.0 | 0.013 | 18.43 |

$a$: Central wavelength for each BATC filter in Å.
$b$: Bandwidth of the filter in Å.
$c$: The number of images that were combined to increase the signal-to-noise ratios in each BATC filter.
$d$: Total exposure time in hours.
$e$: The zero-point errors in magnitude for each filter obtained from the standard stars.
$f$: The limiting magnitudes for S/N=5.

### 3.2 Calibrations of M31–2 to M31–7 Fields

For the images of the M31–2 to M31–7 fields, we performed the same imaging reduction and combination as we did in Section 3.1. The absolute flux of the combined images of the M31–2 to M31–7 fields was calibrated based on secondary standard transformations using the M31–1 field; we could easily identify the stars in common between the M31–2 to M31–7 fields and the M31–1 field, since adjacent overlapping fields were initially arranged. On the image of each filter, we first identified the positions

of the common stars in the overlapping fields, calculated the mean magnitude offsets between the standardized magnitudes and instrumental magnitudes, and then applied this magnitude offset to transform the instrumental magnitudes of the M31–2 to M31–7 fields to the standardized magnitudes.

### 3.3 IRAF/DAOPHOT Photometry

For each M31 GC and GC candidate, the PHOT routine in DAOPHOT (Stetson 1987) is used to obtain magnitudes. To avoid contamination from nearby objects, we adopt an aperture with a radius of 3 pixels on the Ford CCD and of a radius of 4 pixels on the E2V CCD. Inner and outer radii for background determination are taken at 8 to 13 pixels for the 2k×2k Ford CCD corresponding to 10 to 17 pixels for the 4k×4k E2V CCD, from the center of the objects. Given the small aperture used for the GC and GC candidate observations, aperture corrections are determined as follows: We use the isolated stars to determine the magnitude difference between a photometric radius of 3 pixels on the Ford CCD images and that of 4 pixels on the E2V CCD images and the full magnitude of these stars in each of the 15 BATC filters. The spectral energy distributions (SEDs) for the GCs and GC candidates are then corrected for this difference in each filter. However, for AU008, since its background is too bright and varies greatly, we adopted an aperture radius of 2 pixels, and the inner and outer radii for background determination are taken at 3 to 6 pixels, respectively. The SEDs for the sample GCs and GC candidates are listed in Table 5. Cols. (2) to (16) give the magnitudes of the 15 BATC passbands observed. The second line for each object gives the $1-\sigma$ errors in magnitudes for the corresponding passband. The errors for each filter are given by DAOPHOT. For some GCs and GC candidates, the magnitudes in some filters could not be obtained due to low signal-to-noise ratio. Figure 2 shows the findings of the sample GCs and GC candidates in this paper in the BATC $g$ band (centered on 5795 Å), obtained with the NAOC 60/90 cm Schmidt telescope.

### 3.4 Transformed Magnitudes in the Broadband System

It is an uncontroverted fact that the photometry in the broadband system is very commonly used in astrophysical studies. In RBC V.3.5, the authors transformed the magnitudes of M31's 605 GCs and GC candidates from Kim et al. (2007) in the Washington $CMT_1$ photometry to ones in the broadband *UBVRI* system based on the equations of Geisler (1996). These GCs and GC candidates were searched on the CCD images observed by Kim et al. (2007) using the KPNO 0.9m telescope. In order to keep consistency with RBC V.3.5, we will transform the magnitudes of the sample GCs and GC candidates obtained in this paper to ones in the broadband $UBVRI$ system. Using Landolt standards and the catalogs of Landolt (1983, 1992) and of Galadí-Enríquez et al. (2000). Zhou et al. (2003) derived the relationships between the BATC intermediate-band system and the $UBVRI$ broad-band system. These relationships are given in Equations (2) and (6) as:

$$U = m_b + 0.6801(m_a - m_b) - 0.8982 \pm 0.143, \quad (2)$$
$$B = m_d + 0.2201(m_c - m_e) + 0.1278 \pm 0.076, \quad (3)$$
$$V = m_g + 0.3292(m_f - m_h) + 0.0476 \pm 0.027, \quad (4)$$
$$R = m_i + 0.1036 \pm 0.055, \quad (5)$$
$$I = m_o + 0.7190(m_n - m_p) - 0.2994 \pm 0.064. \quad (6)$$
$$(7)$$

$1-\sigma$ errors of the magnitudes were estimated using the formulae below,

$$\sigma_U = \sqrt{{\sigma_b}^2 + 0.6801^2(\sigma_a^2 + \sigma_b^2)}, \quad (8)$$
$$\sigma_B = \sqrt{{\sigma_d}^2 + 0.2201^2(\sigma_c^2 + \sigma_e^2)}, \quad (9)$$
$$\sigma_V = \sqrt{{\sigma_g}^2 + 0.3292^2(\sigma_f^2 + \sigma_h^2)}, \quad (10)$$

**Table 5** Spectral Energy Distributions for 30 Objects in the M31 Field

| ID | $a$ | $b$ | $c$ | $d$ | $e$ | $f$ | $g$ | $h$ | $i$ | $j$ | $k$ | $m$ | $n$ | $o$ | $p$ |
|---|---|---|---|---|---|---|---|---|---|---|---|---|---|---|---|
| (1) | (2) | (3) | (4) | (5) | (6) | (7) | (8) | (9) | (10) | (11) | (12) | (13) | (14) | (15) | (16) |
| B189D | 18.98 | 18.31 | 18.18 | 17.90 | 18.00 | 18.01 | 17.91 | 17.87 | 17.78 | 17.74 | 17.96 | 17.85 | 18.15 | 17.95 | 17.78 |
| | 0.106 | 0.050 | 0.064 | 0.088 | 0.061 | 0.058 | 0.066 | 0.062 | 0.053 | 0.068 | 0.144 | 0.098 | 0.169 | 0.262 | 0.260 |
| B193D | ... | 19.03 | 18.64 | 18.15 | 18.05 | 17.86 | 17.51 | 17.66 | 17.40 | 17.39 | 17.33 | 17.03 | 17.36 | 17.41 | 17.43 |
| | ... | 0.150 | 0.098 | 0.174 | 0.192 | 0.157 | 0.164 | 0.131 | 0.105 | 0.135 | 0.150 | 0.112 | 0.184 | 0.216 | 0.268 |
| G289 | 15.70 | 14.55 | 13.70 | 13.12 | 12.56 | 12.48 | 12.15 | 12.07 | 11.94 | 11.75 | 11.61 | 11.63 | 11.73 | 11.68 | 11.64 |
| | 0.007 | 0.005 | 0.002 | 0.001 | 0.002 | 0.002 | 0.002 | 0.002 | 0.001 | 0.002 | 0.002 | 0.001 | 0.002 | 0.001 | 0.002 |
| G295 | 13.80 | 12.91 | 12.39 | 11.90 | 11.72 | 11.70 | 11.55 | 11.56 | 11.55 | 11.36 | 11.28 | 11.34 | 11.48 | 11.53 | 11.55 |
| | 0.003 | 0.001 | 0.001 | 0.001 | 0.001 | 0.001 | 0.001 | 0.001 | 0.001 | 0.002 | 0.002 | 0.001 | 0.002 | 0.001 | 0.002 |
| NB34 | ... | 20.02 | ... | 18.88 | ... | 17.76 | ... | ... | 17.20 | 17.47 | ... | ... | ... | 17.10 | ... |
| | ... | 0.454 | ... | 0.366 | ... | 0.160 | ... | ... | 0.179 | 0.300 | ... | ... | ... | 0.346 | ... |
| NB61 | ... | ... | ... | ... | ... | ... | ... | ... | 18.48 | 17.70 | 16.78 | 16.69 | 16.47 | 16.12 | 16.07 |
| | ... | ... | ... | ... | ... | ... | ... | ... | 0.760 | 0.438 | 0.225 | 0.245 | 0.232 | 0.175 | 0.177 |
| AU008 | ... | 19.64 | ... | 17.85 | 17.52 | 17.44 | 17.99 | 17.40 | 17.02 | 17.01 | ... | ... | ... | ... | ... |
| | ... | 0.313 | ... | 0.220 | 0.232 | 0.250 | 0.568 | 0.369 | 0.306 | 0.363 | ... | ... | ... | ... | ... |
| AU010 | 19.99 | 19.10 | 19.07 | 18.09 | 17.73 | 17.53 | 17.18 | 16.95 | 16.53 | 16.32 | 15.98 | 15.77 | ... | 15.46 | 15.46 |
| | 0.693 | 0.637 | 1.424 | 0.867 | 0.841 | 0.758 | 0.776 | 0.657 | 0.498 | 0.457 | 0.401 | 0.372 | ... | 0.350 | 0.362 |
| DAO16 | 20.69 | 19.55 | ... | 18.54 | ... | ... | 18.38 | 18.33 | ... | ... | ... | ... | ... | ... | ... |
| | 0.342 | 0.068 | ... | 0.122 | ... | ... | 0.073 | 0.056 | ... | ... | ... | ... | ... | ... | ... |
| DAO23 | 21.10 | 20.49 | 20.11 | 19.41 | 19.45 | 19.47 | 19.16 | 19.18 | 19.29 | 19.13 | 19.48 | 19.32 | 19.74 | 19.11 | 19.93 |
| | 0.345 | 0.119 | 0.161 | 0.190 | 0.116 | 0.075 | 0.096 | 0.102 | 0.079 | 0.093 | 0.320 | 0.179 | 0.414 | 0.362 | 1.132 |
| DAO30 | 20.45 | 19.34 | 18.93 | 18.37 | 18.63 | 18.39 | 18.09 | 17.99 | 17.85 | 17.83 | 17.90 | 17.72 | 17.89 | 17.95 | 18.32 |
| | 0.374 | 0.088 | 0.094 | 0.107 | 0.083 | 0.049 | 0.057 | 0.043 | 0.031 | 0.043 | 0.116 | 0.049 | 0.106 | 0.190 | 0.359 |
| DAO40 | 18.22 | 17.55 | 17.80 | 17.87 | 17.64 | ... | 17.94 | 17.92 | 16.67 | ... | 17.66 | 17.61 | 17.78 | 17.19 | 17.35 |
| | 0.058 | 0.031 | 0.051 | 0.092 | 0.050 | ... | 0.076 | 0.070 | 0.025 | ... | 0.125 | 0.072 | 0.127 | 0.129 | 0.193 |
| DAO46 | 20.13 | 19.54 | 19.28 | 18.61 | 18.84 | 18.70 | 18.55 | 18.39 | 18.24 | 18.25 | 18.11 | 18.13 | 18.06 | 18.16 | 18.23 |
| | 0.260 | 0.100 | 0.133 | 0.133 | 0.097 | 0.060 | 0.070 | 0.056 | 0.039 | 0.052 | 0.140 | 0.071 | 0.125 | 0.241 | 0.376 |
| DAO47 | 20.24 | 19.23 | 19.03 | 18.60 | 18.90 | 18.84 | 18.90 | 19.01 | 18.76 | 18.64 | 18.72 | 18.46 | 18.48 | 18.09 | 18.08 |
| | 0.319 | 0.094 | 0.119 | 0.136 | 0.115 | 0.083 | 0.133 | 0.125 | 0.104 | 0.125 | 0.258 | 0.127 | 0.195 | 0.273 | 0.325 |
| DAO51 | 19.65 | 18.51 | 18.22 | 17.44 | 17.17 | 16.94 | 16.73 | 16.52 | 16.31 | 16.24 | 16.14 | 15.96 | 16.07 | 15.92 | 15.74 |
| | 0.164 | 0.035 | 0.043 | 0.053 | 0.028 | 0.017 | 0.020 | 0.015 | 0.009 | 0.013 | 0.032 | 0.013 | 0.025 | 0.043 | 0.052 |
| DAO53 | ... | 21.07 | 20.12 | 19.81 | 19.40 | 19.08 | 18.70 | 18.58 | 18.24 | 18.24 | 18.11 | 17.97 | 17.85 | 17.86 | 17.79 |
| | ... | 0.426 | 0.303 | 0.422 | 0.170 | 0.088 | 0.099 | 0.071 | 0.039 | 0.074 | 0.145 | 0.060 | 0.098 | 0.200 | 0.255 |
| DAO54 | 21.05 | 20.30 | 19.78 | 19.12 | 18.69 | 18.61 | 18.20 | 18.13 | 17.81 | 17.81 | 17.63 | 17.63 | 17.46 | 17.36 | 17.18 |
| | 0.593 | 0.190 | 0.204 | 0.195 | 0.082 | 0.051 | 0.058 | 0.045 | 0.023 | 0.036 | 0.087 | 0.041 | 0.059 | 0.118 | 0.146 |
| DAO69 | 18.75 | 17.91 | 17.70 | 17.83 | 18.25 | 17.77 | 17.84 | 18.15 | 17.68 | 17.92 | 18.25 | 17.55 | 18.03 | 17.99 | 17.67 |
| | 0.119 | 0.043 | 0.039 | 0.045 | 0.093 | 0.100 | 0.063 | 0.099 | 0.046 | 0.070 | 0.143 | 0.055 | 0.128 | 0.184 | 0.246 |
| DAO84 | ... | 19.81 | 19.42 | 19.25 | 19.26 | 19.39 | 19.11 | 18.75 | 18.48 | 18.89 | 18.71 | 18.50 | 18.54 | 18.30 | 18.69 |
| | ... | 0.294 | 0.070 | 0.186 | 0.145 | 0.137 | 0.140 | 0.077 | 0.074 | 0.147 | 0.168 | 0.108 | 0.266 | 0.168 | 1.008 |
| V202 | 20.42 | 19.04 | 18.98 | 19.03 | 19.13 | ... | 19.38 | 19.67 | ... | ... | ... | ... | ... | ... | ... |
| | 0.286 | 0.076 | 0.087 | 0.115 | 0.169 | ... | 0.344 | 0.474 | ... | ... | ... | ... | ... | ... | ... |
| V203 | 19.07 | 18.98 | 19.18 | 19.38 | 17.23 | ... | ... | ... | 17.07 | ... | ... | ... | ... | 18.28 | ... |
| | 0.075 | 0.251 | 0.083 | 0.103 | 0.016 | ... | ... | ... | 0.023 | ... | ... | ... | ... | 0.126 | ... |
| V226 | 20.82 | 19.34 | 20.01 | 19.84 | 18.66 | 19.54 | 19.60 | 19.84 | 17.14 | 19.25 | 19.44 | 19.60 | ... | 17.57 | ... |
| | 0.339 | 0.293 | 0.086 | 0.083 | 0.034 | 0.084 | 0.105 | 0.112 | 0.019 | 0.127 | 0.174 | 0.216 | ... | 0.064 | ... |
| V234 | 19.09 | 18.55 | 18.15 | 17.96 | 17.74 | 17.59 | 17.33 | 17.33 | 16.86 | 17.08 | 16.87 | 16.67 | 16.47 | 16.44 | 16.45 |
| | 0.077 | 0.154 | 0.038 | 0.041 | 0.053 | 0.052 | 0.063 | 0.058 | 0.057 | 0.071 | 0.074 | 0.080 | 0.080 | 0.086 | 0.095 |
| V245 | 18.91 | 19.24 | 18.77 | 19.26 | 18.51 | 19.90 | 21.47 | ... | 17.13 | ... | ... | ... | ... | ... | ... |
| | 0.081 | 0.291 | 0.040 | 0.051 | 0.012 | 0.025 | 0.059 | ... | 0.009 | ... | ... | ... | ... | ... | ... |
| BA28 | ... | 20.67 | 20.17 | 19.68 | 19.68 | 19.48 | 18.65 | 18.58 | 18.32 | 18.35 | 17.80 | 17.94 | 17.80 | 17.74 | 18.69 |
| | ... | 0.453 | 0.285 | 0.222 | 0.269 | 0.649 | 0.129 | 0.090 | 0.045 | 0.096 | 0.086 | 0.071 | 0.109 | 0.145 | 0.665 |
| SH07 | 18.49 | 17.57 | 17.66 | 17.41 | 17.05 | 16.85 | 16.63 | 16.55 | 16.34 | 16.35 | 16.23 | 16.02 | 16.03 | 15.98 | 15.88 |
| | 0.075 | 0.024 | 0.013 | 0.056 | 0.030 | 0.017 | 0.026 | 0.013 | 0.020 | 0.037 | 0.016 | 0.015 | 0.029 | 0.045 | 0.045 |
| BH10 | ... | 20.49 | 20.31 | 19.29 | 19.29 | 19.39 | 18.91 | 18.70 | 18.69 | 18.77 | 18.85 | 18.60 | 19.06 | 18.43 | 18.70 |
| | ... | 0.300 | 0.422 | 0.263 | 0.193 | 0.182 | 0.173 | 0.130 | 0.119 | 0.156 | 0.362 | 0.177 | 0.401 | 0.393 | 0.644 |
| B515 | ... | 19.93 | 19.77 | 19.16 | 18.70 | 18.65 | 18.37 | 18.20 | ... | 17.87 | 17.87 | 17.73 | ... | 17.66 | ... |
| | ... | 0.394 | 0.074 | 0.042 | 0.037 | 0.033 | 0.052 | 0.036 | ... | 0.057 | 0.072 | 0.076 | ... | 0.074 | ... |
| B521 | ... | 19.72 | 19.71 | 19.87 | 19.23 | 18.96 | 19.00 | 19.00 | 18.68 | 18.67 | 18.61 | 18.43 | 18.30 | 17.90 | 17.72 |
| | ... | 0.130 | 0.214 | 0.379 | 0.158 | 0.101 | 0.141 | 0.130 | 0.094 | 0.119 | 0.228 | 0.109 | 0.154 | 0.197 | 0.235 |
| B524 | ... | ... | 19.99 | 20.03 | 19.71 | 19.88 | 19.21 | 19.28 | 19.42 | 18.91 | 19.19 | 18.95 | 18.25 | 18.49 | 18.40 |
| | ... | ... | 0.274 | 0.218 | 0.160 | 0.206 | 0.136 | 0.117 | 0.205 | 0.138 | 0.235 | 0.210 | 0.148 | 0.184 | 0.248 |

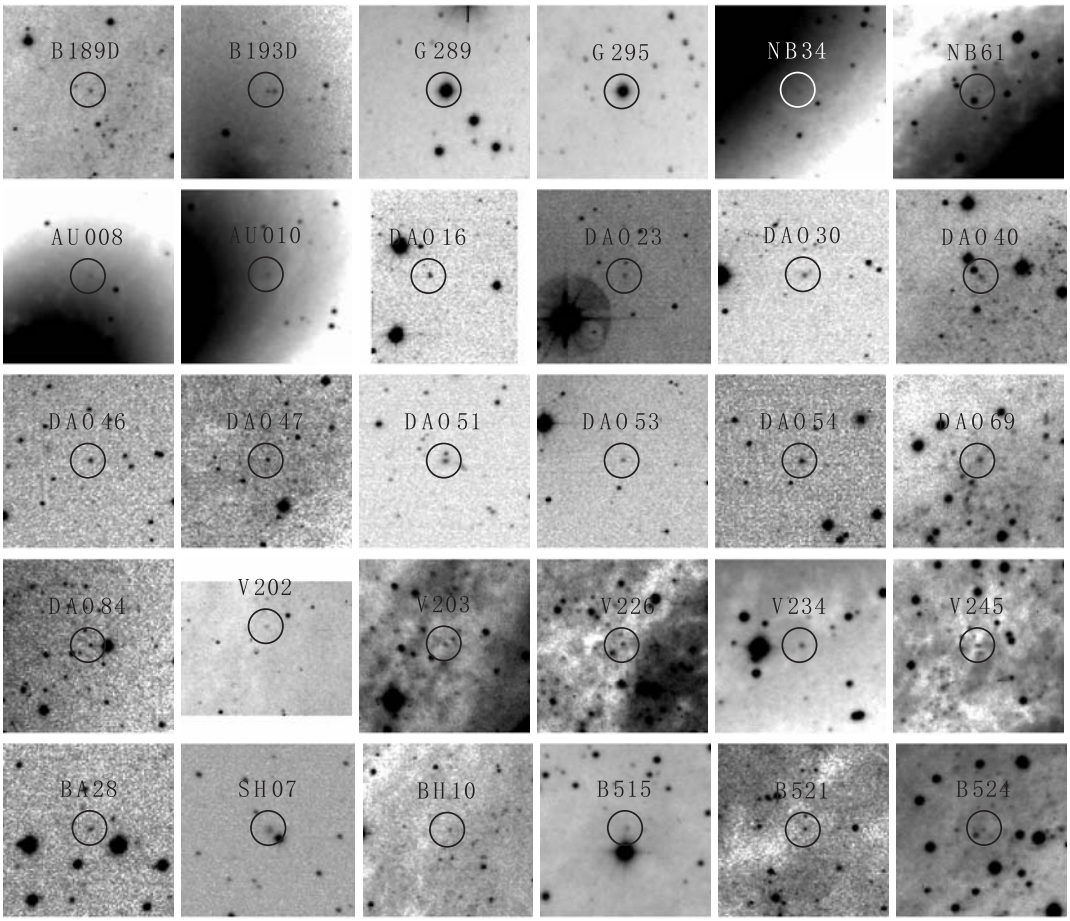


**Fig. 2** Images of the sample GC candidates in the BATC $g$ band obtained with the NAOC 60/90 cm Schmidt telescope, which are circled. The field of view of the image is $2.8 \times 2.8$ arcmin$^2$.

$$\sigma_R = \sigma_i, \tag{11}$$

$$\sigma_I = \sqrt{{\sigma_o}^2 + 0.7190^2(\sigma_n^2 + \sigma_p^2)}. \tag{12}$$

Using these equations, we calculate the $UBVRI$ broadband magnitudes and $1-\sigma$ errors for the GCs and GC candidates in this paper and list them in Table 6.

## 4 RESULTS AND DISCUSSION

### 4.1 Comparison of the Broadband Magnitude

Very recently, Caldwell et al. (2009) presented an updated catalog for 1300 objects in M31, including 670 likely star clusters. This catalog presented the magnitudes in the $V$ band for most objects based on the observations of the LGS survey of M31. In order to check the photometry in this paper, we compared the results between Caldwell et al. (2009) and this paper. In Figure 3, we plot the comparison of $V$ (BATC) photometry with the measurement of Caldwell et al. (2009). In this figure, our magnitudes are on the $x$-axis, the difference between our magnitudes and those from Caldwell et al. (2009) are shown

**Table 6** Broadband $UBVRI$ Magnitudes of GCs and Candidates Derived from the BATC 15-Band Photometry in Our Sample

| ID (1) | $U$ (2) | $\sigma_U$ (3) | $B$ (4) | $\sigma_B$ (5) | $V$ (6) | $\sigma_V$ (7) | $R$ (8) | $\sigma_R$ (9) | $I$ (10) | $\sigma_I$ (11) |
|---|---|---|---|---|---|---|---|---|---|---|
| B189D | 17.87 | 0.094 | 18.07 | 0.090 | 18.01 | 0.072 | 17.88 | 0.053 | 17.92 | 0.344 |
| B193D | ... | ... | 18.40 | 0.180 | 17.62 | 0.177 | 17.50 | 0.105 | 17.06 | 0.318 |
| G289 | 14.43 | 0.008 | 13.50 | 0.001 | 12.33 | 0.002 | 12.04 | 0.001 | 11.44 | 0.002 |
| G295 | 12.61 | 0.002 | 12.18 | 0.001 | 11.64 | 0.001 | 11.65 | 0.001 | 11.18 | 0.002 |
| NB34 | ... | ... | ... | ... | ... | ... | 17.31 | 0.179 | ... | ... |
| NB61 | ... | ... | ... | ... | ... | ... | 18.58 | 0.760 | 16.11 | 0.273 |
| AU008 | ... | ... | ... | ... | 18.05 | 0.587 | 17.13 | 0.306 | ... | ... |
| AU010 | 18.81 | 0.903 | 18.52 | 0.940 | 17.42 | 0.843 | 16.63 | 0.498 | ... | ... |
| DAO16 | 19.43 | 0.247 | ... | ... | ... | ... | ... | ... | ... | ... |
| DAO23 | 20.01 | 0.275 | 19.68 | 0.195 | 19.30 | 0.105 | 19.40 | 0.079 | 18.68 | 0.939 |
| DAO30 | 19.20 | 0.276 | 18.56 | 0.111 | 18.27 | 0.061 | 17.95 | 0.031 | 17.34 | 0.329 |
| DAO40 | 17.11 | 0.054 | 18.03 | 0.093 | ... | ... | 16.78 | 0.025 | 17.20 | 0.210 |
| DAO46 | 19.04 | 0.214 | 18.83 | 0.138 | 18.70 | 0.075 | 18.35 | 0.039 | 17.74 | 0.373 |
| DAO47 | 19.02 | 0.245 | 18.76 | 0.141 | 18.89 | 0.142 | 18.86 | 0.104 | 18.09 | 0.386 |
| DAO51 | 18.39 | 0.119 | 17.80 | 0.054 | 16.91 | 0.021 | 16.41 | 0.009 | 15.86 | 0.060 |
| DAO53 | ... | ... | 20.10 | 0.429 | 18.91 | 0.106 | 18.34 | 0.039 | 17.60 | 0.280 |
| DAO54 | 19.91 | 0.464 | 19.49 | 0.201 | 18.41 | 0.062 | 17.91 | 0.023 | 17.25 | 0.164 |
| DAO69 | 17.58 | 0.096 | 17.84 | 0.050 | 17.76 | 0.078 | 17.78 | 0.046 | 17.95 | 0.271 |
| DAO84 | ... | ... | 19.41 | 0.189 | 19.37 | 0.149 | 18.58 | 0.074 | 17.89 | 0.768 |
| V202 | 19.08 | 0.215 | 19.13 | 0.122 | ... | ... | ... | ... | ... | ... |
| V203 | 18.14 | 0.308 | 19.94 | 0.105 | ... | ... | 17.17 | 0.023 | ... | ... |
| V226 | 19.45 | 0.423 | 20.26 | 0.085 | 19.55 | 0.115 | 17.25 | 0.019 | ... | ... |
| V234 | 18.02 | 0.193 | 18.18 | 0.043 | 17.47 | 0.068 | 16.96 | 0.057 | 16.16 | 0.124 |
| V245 | 18.12 | 0.356 | 19.44 | 0.052 | ... | ... | 17.23 | 0.009 | ... | ... |
| BA28 | ... | ... | 19.91 | 0.238 | 18.99 | 0.251 | 18.42 | 0.045 | 16.80 | 0.506 |
| SH07 | 17.30 | 0.059 | 17.67 | 0.056 | 16.78 | 0.027 | 16.44 | 0.020 | 15.79 | 0.059 |
| BH10 | ... | ... | 19.64 | 0.282 | 19.19 | 0.188 | 18.80 | 0.119 | 18.39 | 0.672 |
| B515 | ... | ... | 19.52 | 0.046 | 18.57 | 0.054 | ... | ... | ... | ... |
| B521 | ... | ... | 20.11 | 0.383 | 19.04 | 0.151 | 18.78 | 0.094 | 18.01 | 0.282 |
| B524 | ... | ... | 20.22 | 0.229 | 19.45 | 0.157 | 19.53 | 0.205 | 18.08 | 0.277 |

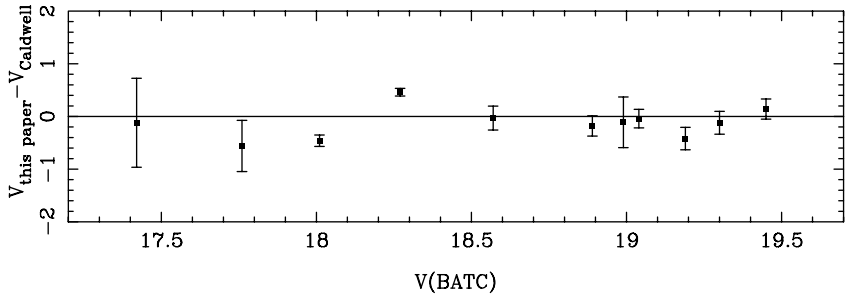


**Fig. 3** Comparison of GC candidate photometry with previous measurements by Caldwell et al. (2009).

on the $y$-axis. The mean $V$ magnitude difference (in the sense of this paper − Caldwell et al. 2009) is $\langle \Delta V \rangle = -0.13 \pm 0.27$.

### 4.2 Magnitude and Color Distributions

Based on the combined photometry of RBC V.3.5 and Table 6 in this paper, Figure 4 plots the *UBVRI* magnitude distributions of M31's confirmed GCs and GC candidates classified in RBC V.3.5. The dis-

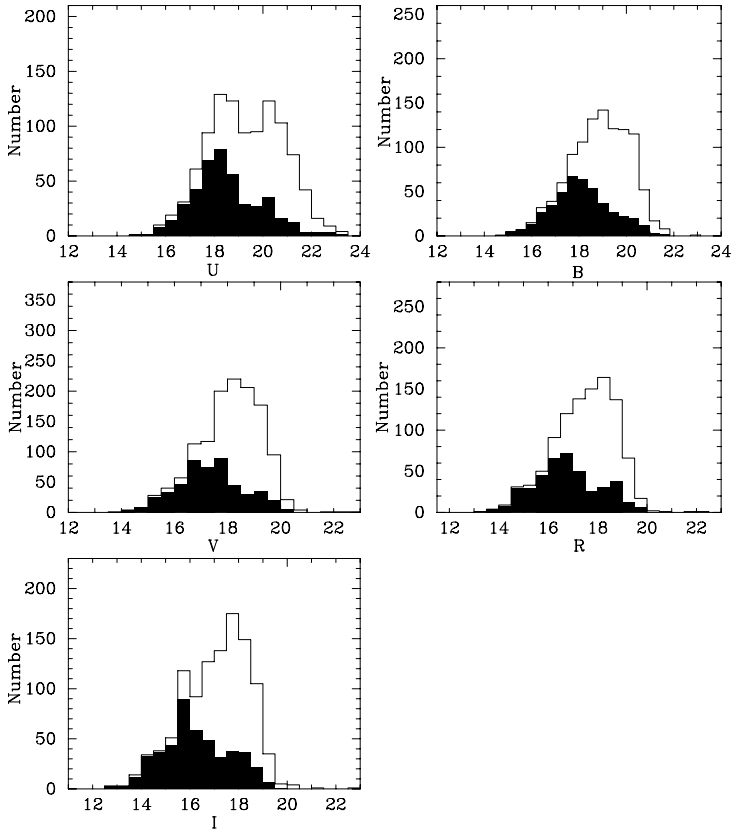


**Fig. 4** Distributions of the magnitudes of M31 GCs and candidates in $U, B, V, R$ and $I$ bands, which combine the photometry from RBC V.3.5 and those from Table 6. The open histograms are for the GCs and GC candidates while the hatched histograms are for the confirmed GCs.

tributions for the confirmed GCs ($f = 1$ in RBC V.3.5) are presented with the hatched histograms while the open histograms are for the GCs and GC candidates ($f = 1$, 2 and 3 in RBC V.3.5)[2]. We indicate that in RBC V.3.5, $f = 1$, 2 and 3 represent confirmed GCs, GC candidates and controversial objects. The controversial objects, the total number of which is only nine in RBC V.3.5, mean that, for example, some objects have been classified as galaxies based on high resolution ground images, while they are classified as GCs on the basis of spectroscopic observations (see Galleti et al. 2004 for more details). They need to be confirmed in the future. They are included as GC candidates in this paper. In all, combining the photometry in RBC V.3.5 and in this paper, there are totally 1029, 1085, 1289, 1033 and 1093 photometric values in the $U, B, V, R$ and $I$ bands for GCs and GC candidates in M31, respectively, and there are 428, 449, 506, 423 and 456 confirmed GCs having photometric data in $U, B, V, R$ and $I$ bands, respectively. Obviously, the confirmed GCs only occupy a small part of the candidates. So, in the future, it is also needed to confirm which GC candidates are actually GCs.

In addition, Figure 5 also plots the color distributions for the GCs and GC candidates with the same photometric data as in Figure 4. For the *bona fide* GCs (the hatched histograms), the peak values of the color distributions in $B-V$, $B-R$, $B-I$, $V-R$, $U-B$ and $V-K$ are about 0.8, 1.3, 1.9, 0.5, 0.3 and 2.5, respectively. The peak values of the color distributions for all the GCs and GC candidates are

[2] Note that there are 265 GC candidates in RBC V.3.5, which are classified as stars (148) and galaxies (117) by Caldwell et al. (2009). So, we did not include these objects in Fig. 4.

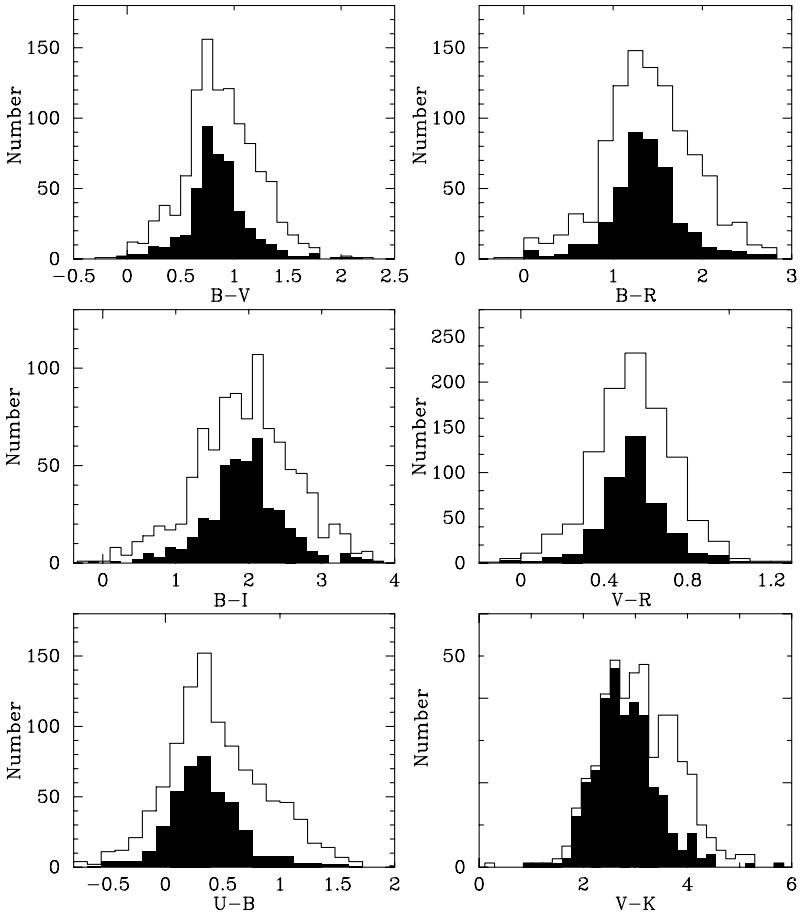


**Fig. 5** Color distributions of M31 GCs and candidates, which combine the photometric data from RBC V.3.5 and this paper. The open solid histograms represent the GCs and candidates while the hatched histograms represent the confirmed GCs.

nearly the same as those of the *bona fide* GCs except for the $V-K$ color. It seems that the confirmed GCs dominate the bluest part of all the GCs and GC candidates in the $V-K$ color distribution while the other color distributions do not show this phenomenon, which is also seen in Figure 6. This may be due to the fact that Near Infrared (NIR) photometry of GCs and GC candidates in RBC V.3.5 is actually lacking, which can be easily seen based on the number of $V-K$ colors. 2MASS is the main source of NIR photometry in RBC V.3.5. However, as the exposure time is usually too short in the 2MASS survey, the NIR photometry of faint GCs and GC candidates is not obtained in RBC V.3.5. In addition, bright GCs are easily searched.

Figure 6 plots the color-color diagrams of GCs and GC candidates in RBC V.3.5: $V-K$ vs various colors, which are from RBC V.3.5 and Table 6. The confirmed GCs are marked with circles while the GC candidates are shown as black pluses. The reason that we use the $V-K$ in every color-color diagram is that $V-K$ can provide a useful discriminant to separate the $bona fide$ GCs from background galaxies (Galleti et al. 2004). In this figure, it is easy to find that most of the $bona\ fide$ GCs with $V-K<3.0$ while most of the $V-K>3.0$ points are GC candidates. Therefore, there are a lot of GC candidates which might be the background galaxies according to the conclusion of Galleti et al. (2004).

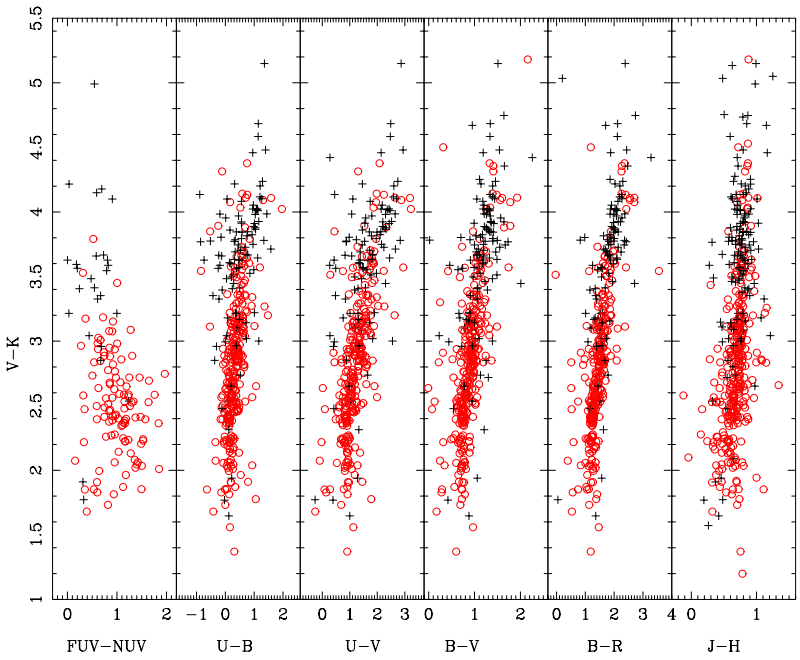


**Fig. 6** Color-color diagrams of GCs and GC candidates: $V - K$ vs. various colors. The photometric data are from RBC V.3.5 and this paper. The circles represent the confirmed GCs while the black pluses represent the GC candidates.

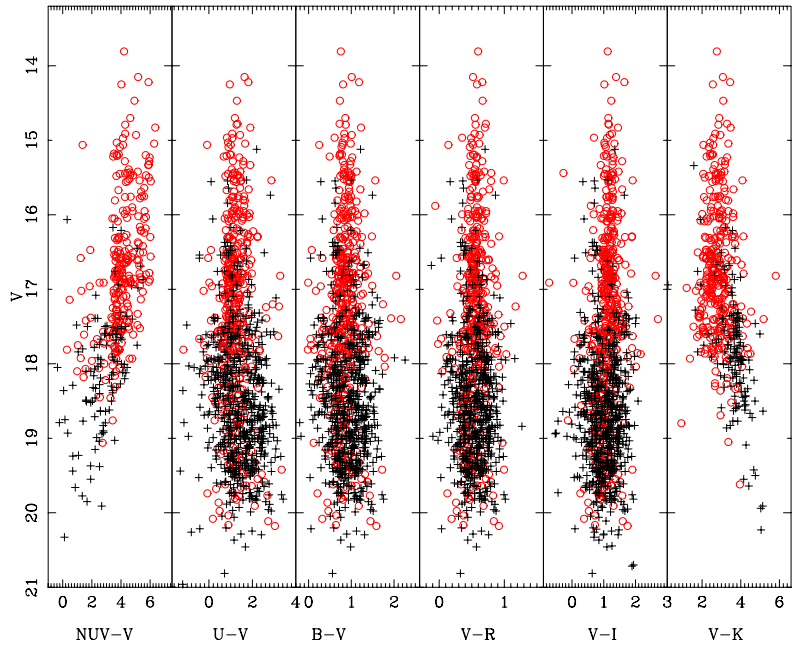


**Fig. 7** Color - $V$ magnitude diagrams for the GCs and GC candidates. The photometric data are from RBC V.3.5 and Table 6. The circles represent the confirmed GCs while the black pluses represent the GC candidates.

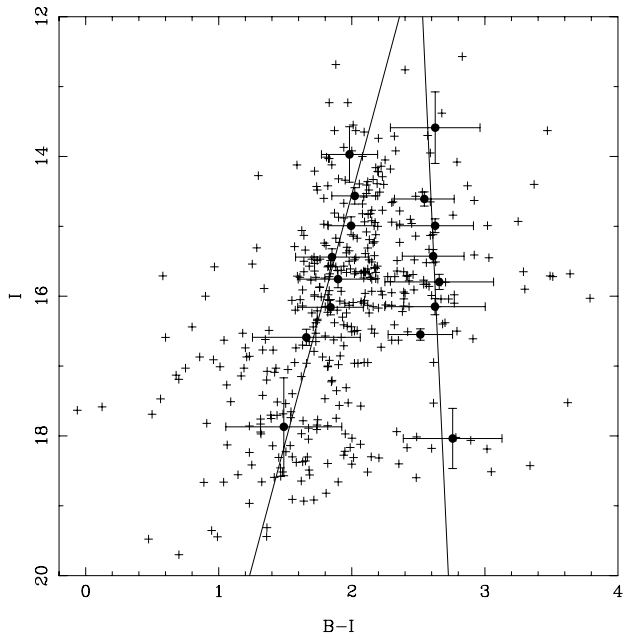


**Fig. 8** $I$ vs. $B-I$ diagram for all the confirmed GCs in M31. The data used are from RBC V.3.5 and this paper. The linear fits show blue tilt for the blue population while there is no such relationship for the red population.

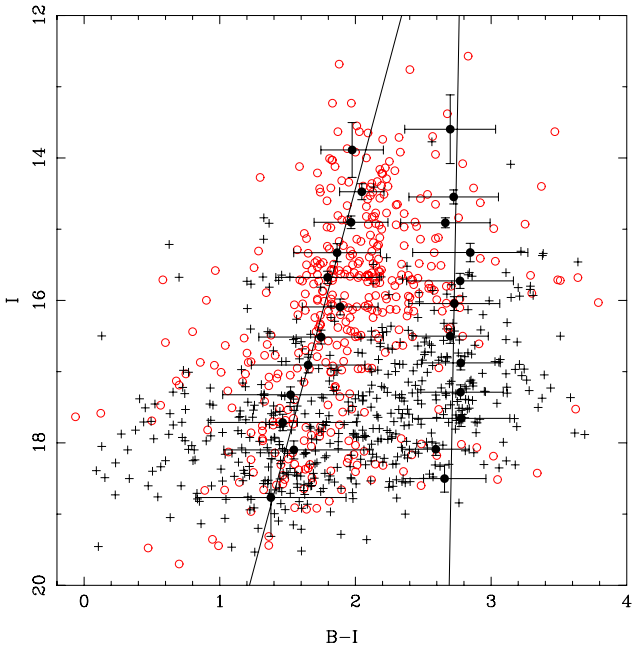


**Fig. 9** The same as Fig. 8, but for all the confirmed GCs (*circles*) and GC candidates (*black pluses*). The data used are also from RBC V.3.5 and this paper. We can also find the blue tilt in this figure.

Figure 7 shows the color-$V$ magnitude diagrams for the GCs and GC candidates. Most of the candidates are fainter than $V = 17$ while most of the bright objects ($V < 17$) are confirmed GCs. This implies that the fainter candidates are difficult to be identified and the bright GCs are much easier to be searched.

### 4.3 The Color - Luminosity Relationship

Harris et al. (2006) investigated the color magnitude diagrams (CMDs) of GCs in eight of the brightest cluster galaxies (BCGs) with the ACS/WFC data of *HST*, and found a trend that the redder GCs are more luminous (massive) for the blue (metal-poor) population with $M_I > -10.5$, which is called "blue tilt." After that, Strader et al. (2006) also found the blue tilt phenomenon in giant ellipticals (gEs) M87 and NGC 4649 in the Virgo Cluster by analyzing the *HST*/ACS images, and used the self-enrichment to interpret this phenomenon. Spitler et al. (2006) also utilized the *HST*/ACS images to study the Sa/S0 galaxy Sombrero (NGC 4594) and found blue tilt in the CMD. Mieske et al. (2006) found that the blue tilt exists in early galaxies from the brightest ones to the faintest ones in the Virgo Cluster with the *HST*/ACS observations, and the slope is deeper in the more luminous host galaxies. Mieske et al. (2006) indicated that self-enrichment and field star capture, or a combination of the two processes, offer the most promising means of explaining the blue tilt. Strader & Smith (2008) analyzed all the possible explanations for the blue tilt phenomenon discovered previously in various external galaxies, and showed that the self-enrichment in proto-GC clouds can reproduce some aspects of the blue tilt. In this model, star formation is controlled by supernova feedback, and the efficiency scaling is proportional to the protocloud mass. Strader & Smith (2008) also investigated the metallicity and mass relationship of Galactic GCs, and did not find the blue tilt; in addition, they suggested that this might be due to the fundamental differences between the parent clouds of Galactic GCs and those in blue-tilt galaxies. However, Strader & Smith (2008) do not know whether the blue tilt exits in M31 or not. We will investigate this phenomenon based on the data in RBC V.3.5 and in this paper.

We plot the CMDs in the $(B - I)$ vs. $I$ band for all the confirmed GCs of M31 in Figure 8 and for all the confirmed GCs and GC candidates of M31 in Figure 9. The KMM mixture modeling routine (Ashman et al. 1994) was performed to distinguish the blue and red subpopulations in both figures. Then, we divided the GCs into several mag bins to calculate the mean color and mean magnitude in each bin (see the big black spots in Figs. 8 and 9). We fit the linear relationship for the color $B - I$ and magnitude $I$ with the formula: $B - I = a + bI$. First, we fit the data of the confirmed GCs; for the blue population, we have $b = -0.141 \pm 0.021$ while for the red population $b = 0.024 \pm 0.020$. Then for all the GCs and GC candidates, we have $b = -0.140 \pm 0.013$ for the blue population and $b = -0.009 \pm 0.014$ for the red population. The results strongly present evidence of significant slopes for the blue population. However, the slopes for the red population nearly approach zero, in other words, the luminosity of the red GC population is completely independent of its color, which means there is no such relationship for the red GC population.

## 5 CONCLUSIONS

In this paper, we obtain the photometry of 30 M31 GCs and GC candidates in 15 BATC intermediate bands. Based on equestions (6) – (10) of Zhou et al. (2003), we transformed the BATC intermediate-band magnitudes to the broadband $UBVRI$ magnitudes for these GCs and GC candidates. We checked the objects in our BATC images and found that 4 objects could not be detected in the locations presented in RBC V.3.5.

We also investigated the relationship between $I$ mag and $B - I$ color for the confirmed GCs, and GCs and GC candidates, respectively. After fitting, we obtained the slope of the blue population $b = -0.141 \pm 0.021$ for the confirmed GCs, and $b = -0.140 \pm 0.013$ for all the GCs and GC candidates.

Finally, we point out that our new supplementary photometry to RBC V.3.5 is not only helpful for us to understand the total nature of GCS in M31 but also useful for the Large Sky Area Multi-Object Fiber Spectroscopic Telescope (LAMOST) project of China to estimate the exposure time when

observing them by LAMOST. LAMOST is being built at Xinglong Station of the National Astronomical Observatory, Chinese Academy of Sciences (NAOC), Heibei province of P. R. China. This telescope is a reflecting Schmidt telescope with an effective aperture of 4 meters and a primary mirror of 6 meters mounted on it which applies active optics and fiber positioning technology. The angular diameter of the field of view (FOV) is 5 degrees and 4000 fibers are in the large focal plane with a 1.75-meter diameter, which makes it possess the ability to produce several tens of thousands of spectra in one night for faint objects down to $V = 20.5$ mag. The LAMOST project has been completed at the end of 2008 and its spectroscopic survey will make important contributions to stellar astrophysics, the Galaxy, extra-galactic astrophysics and cosmology (Zhao 1999). Thus, it is proper to use LAMOST to investigate properties of GCs and GC candidates in M31 because of its wide FOV ($5^\circ$). Hundreds of star clusters can be observed at the same time.

LAMOST is appropriate for studying the properties of M31 GCs and GC candidates: in a few good nights, the spectral observations of M31 GCs and GC candidates can be obtained. Based on these data, we can study the properties of M31 GCs and GC candidates, such as confirming GCs with radial velocities and determining metallicities by measuring the strengths of various absorption features in the integrated spectra (see Perrett et al. 2002, and references there).

**Acknowledgements** We are indebted to the referee for thoughtful comments and insightful suggestions that improved this paper greatly. This work is supported by the National Natural Science Foundation of China (Grant Nos. 10873016, 10803007, 10473012, 10573020, 10633020, 10673012 and 10603006); and by the National Basic Research Program of China (973 Program, No. 2007CB815403).

## References

Ashman, K. M., Bird, C. M., & Zepf, S. E. 1994, AJ, 108, 2348
Barmby, P., Huchra, J., Brodie, J., Forbes, D., Schroder, L., & Grillmair, C. 2000, AJ, 119, 727
Battistini, P., Bònoli, F., Braccesi, A., Fusi Pecci, F., Malagnini, M. L., & Marano, B. 1980, A&AS, 42, 357
Battistini, P., Bònoli, F., Braccesi, A., Federici, L., Fusi Pecci, F., Marano, B., & Börngen, F. 1987, A&AS, 67, 447
Battistini, P., Bònoli, F., Casavecchia, M., Ciotti, L., Federici, L., & Fusi Pecci, F. 1993, A&A, 272, 77
Baum, W. A., et al. 1995, AJ, 110, 2537
Caldwell, N., Harding, P., Morrison, H., Rose, J. A., Schiavon, R., & Kriessler, J. 2009, AJ, 137, 94
Crampton, D., Cowley, A. P., Schade, D., & Chayer, P. 1985, ApJ, 288, 494
Fan, X.-H., et al. 1996, AJ, 112, 628
Fukugita, M., et al. 1996, AJ, 111, 1748
Galadí-Enríquez, D., Trullols, E., & Jordi, C. 2000, A&AS, 146, 169
Galleti, S., Federici, L., Bellazzini, M., Fusi Pecci, F., & Macrina, S. 2004, A&A , 416, 917
Galleti, S., Bellazzini, M., Federici, L., & Fusi Pecci, F. 2005, A&A, 436, 535
Galleti, S., Federici, L., Bellazzini, M., Buzzoni, A., & Fusi Pecci, F. 2006, A&A, 456, 985
Galleti, S., Bellazzini, M., Federici, L., Buzzoni, A., & Fusi Pecci, F. 2007, A&A, 471, 127
Geisler, D. 1996, AJ, 111, 480
Harris, W. E., et al. 2006, ApJ, 636, 90
Huxor, A. P., Tanvir, N. R., Ferguson, A. M. N., Irwin, M. J., Ibata, R., Bridges, T., & Lewis, G. F. 2008, MNRAS, 385, 1989
Jiang, L.-H., Ma, J., Zhou, X., Chen, J.-S., Wu, H., & Jiang, Z.-J. 2003, AJ, 125, 727
Kalirai, J. S., Strader, J., Anderson, J., & Bicher, H. B. 2008, ApJ, 682, L37
Kim, S. C., Lee, M. G., Geisler, D., Sarajedini, A., Park, H. S., Hwang, H. S., Harris, W. E., Seguel, J. C., & von Hippel, T. 2007, AJ, 134, 706
Landolt, A. U. 1983, AJ, 88, 439
Landolt, A. U. 1992, AJ, 104, 340
Ma, J., et al. 2006a, PASP, 118, 98
Ma, J., et al. 2006b, A&A, 449, 143
Ma, J., et al. 2006c, MNRAS, 368, 1443

Ma, J., et al. 2007, ApJ, 659, 359
Mackey, A. D., Huxor, A., Ferguson, A. M. N., Tanvir, N. R., Irwin, M., Ibata, R., Bridges, T., Johnson, R. A., & Lewis, G. 2006, ApJ, 653, L105
Macri, L. M., et al. 2001, ApJ, 549, 721
Massey, P., Olsen, K. A. G., Hodge, P. W., Strong, S. B., Jacoby, G. H., Schlingman, W., & Smith, R. C. 2006, AJ, 131, 2478
McConnachie, A. W., Irwin, M. J., Ferguson, A. M. N., Ibata, R. A., Lewis, G. F., & Tanvir, N. 2005, MNRAS, 356, 979
Mieske, S., et al. 2004, AJ, 128, 1529
Mieske, S., et al. 2006, ApJ, 653, 193
Oke, J. B., & Gunn, J. E. 1983, ApJ, 266, 713
Peng, E. W., et al. 2006, ApJ, 639, 95
Perrett, K. M., Bridges, T. J., Hanes, D. A., Irwin, M. J., Brodie, J. P., Carter, D., Huchra, J. P., & Watson, F. G. 2002, AJ, 123, 2490
Racine, R. 1991, AJ, 101, 865
Sargent, W. L. W., Kowal, C. T., Hartwick, F. D. A., & van den Bergh, S. 1977, AJ, 82, 947
Spitler, L. R., et al. 2006, AJ, 132, 1593
Stanek, K. Z., & Garnavich, P. M. 1998, ApJ, 503, L131
Stetson, P. B. 1987, PASP, 99, 191
Strader, J., Brodie, J. P., Spitler, L., & Beasley, M. A. 2006, AJ, 132, 2333
Strader, J., & Smith, G. H. 2008, AJ, 136, 1828
Vetesnik, M. 1962, Bulletin of the Astronomical Institutes of Czechoslovakia, 13, 180
Wu, H., et al. 2002, AJ, 123, 1364
Yan, H.-J., et al. 2000, PASP, 112, 691
Yi, S. K. 2009, (arXiv:0903.2891)
Zhao, Y.-H. 1999, Observational Astrophysics in Asia and its Future, 1
Zheng, Z.-Y., et al. 1999, AJ, 117, 2757
Zhou, X., Jiang, Z.-J., Xue, S.-J., Wu, H., Ma, J., & Chen, J.-S. 2001, ChJAA (Chin. J. Astron. Astrophys.), 1, 372
Zhou, X., et al. 2003, A&A, 397, 361
Zhou, X., et al. 2004, AJ, 127, 3642